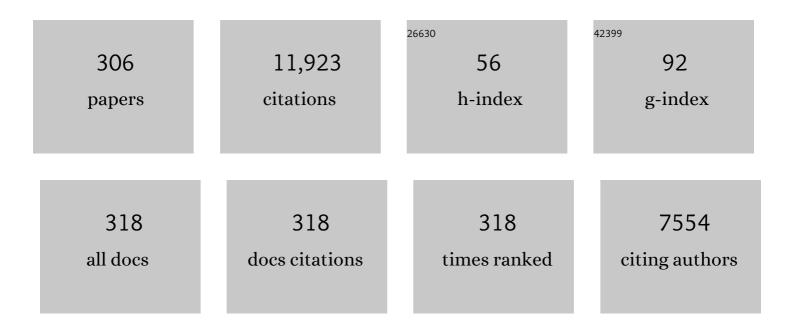
Nikhilesh Chawla

List of Publications by Year in descending order

Source: https://exaly.com/author-pdf/4539893/publications.pdf Version: 2024-02-01



#	Article	IF	CITATIONS
1	Mechanical Behavior of Particle Reinforced Metal Matrix Composites. Advanced Engineering Materials, 2001, 3, 357-370.	3.5	628
2	Tensile behavior of high performance natural (sisal) fibers. Composites Science and Technology, 2008, 68, 3438-3443.	7.8	318
3	Deformation behavior of (Cu, Ag)–Sn intermetallics by nanoindentation. Acta Materialia, 2004, 52, 4291-4303.	7.9	284
4	Microstructure and mechanical behavior of porous sintered steels. Materials Science & Engineering A: Structural Materials: Properties, Microstructure and Processing, 2005, 390, 98-112.	5.6	277
5	Three-dimensional visualization and microstructure-based modeling of deformation in particle-reinforced composites. Acta Materialia, 2006, 54, 1541-1548.	7.9	242
6	Effect of SiC volume fraction and particle size on the fatigue resistance of a 2080 Al/SiC p composite. Metallurgical and Materials Transactions A: Physical Metallurgy and Materials Science, 1998, 29, 2843-2854.	2.2	224
7	Microstructure and deformation behavior of biocompatible TiO2 nanotubes on titanium substrateâ~†. Acta Biomaterialia, 2007, 3, 359-367.	8.3	220
8	Three-dimensional (3D) microstructure visualization and finite element modeling of the mechanical behavior of SiC particle reinforced aluminum composites. Scripta Materialia, 2004, 51, 161-165.	5.2	198
9	Creep deformation behavior of Sn–3.5Ag solder/Cu couple at small length scales. Acta Materialia, 2004, 52, 4527-4535.	7.9	196
10	Effects of cooling rate on the microstructure and tensile behavior of a Sn-3.5wt.%Ag solder. Journal of Electronic Materials, 2003, 32, 1414-1420.	2.2	180
11	Metal-matrix composites in ground transportation. Jom, 2006, 58, 67-70.	1.9	176
12	Influence of reflow and thermal aging on the shear strength and fracture behavior of Sn-3.5Ag solder/Cu joints. Metallurgical and Materials Transactions A: Physical Metallurgy and Materials Science, 2005, 36, 55-64.	2.2	162
13	Effect of particle orientation anisotropy on the tensile behavior of metal matrix composites: experiments and microstructure-based simulation. Materials Science & Engineering A: Structural Materials: Properties, Microstructure and Processing, 2005, 391, 342-353.	5.6	155
14	Young's modulus of (Cu, Ag)–Sn intermetallics measured by nanoindentation. Materials Science & Engineering A: Structural Materials: Properties, Microstructure and Processing, 2004, 364, 240-243.	5.6	153
15	Influence of initial morphology and thickness of Cu6Sn5 and Cu3Sn intermetallics on growth and evolution during thermal aging of Sn-Ag solder/Cu joints. Journal of Electronic Materials, 2003, 32, 1403-1413.	2.2	143
16	Microstructure-based modeling of the deformation behavior of particle reinforced metal matrix composites. Journal of Materials Science, 2006, 41, 913-925.	3.7	128
17	The influence of microencapsulated phase change material (PCM) characteristics on the microstructure and strength of cementitious composites: Experiments and finite element simulations. Cement and Concrete Composites, 2016, 73, 29-41.	10.7	128
18	Damage evolution in SiC particle reinforced Al alloy matrix composites by X-ray synchrotron tomography. Acta Materialia, 2010, 58, 6194-6205.	7.9	124

#	Article	IF	CITATIONS
19	Metal Matrix Composites. , 2013, , .		119
20	Microstructure-based modeling of crack growth in particle reinforced composites. Composites Science and Technology, 2006, 66, 1980-1994.	7.8	118
21	Microstructure-based simulation of thermomechanical behavior of composite materials by object-oriented finite element analysis. Materials Characterization, 2002, 49, 395-407.	4.4	114
22	Mechanical properties of Cu6Sn5 intermetallic by micropillar compression testing. Scripta Materialia, 2010, 63, 480-483.	5.2	111
23	Effective properties of a fly ash geopolymer: Synergistic application of X-ray synchrotron tomography, nanoindentation, and homogenization models. Cement and Concrete Research, 2015, 78, 252-262.	11.0	107
24	Correlation between tensile and indentation behavior of particle-reinforced metal matrix composites: an experimental and numerical study. Acta Materialia, 2001, 49, 3219-3229.	7.9	106
25	Effects of cooling rate on creep behavior of a Sn-3.5Ag alloy. Journal of Electronic Materials, 2004, 33, 1596-1607.	2.2	104
26	Three dimensional (3D) microstructure-based modeling of interfacial decohesion in particle reinforced metal matrix composites. Materials Science & Engineering A: Structural Materials: Properties, Microstructure and Processing, 2012, 557, 113-118.	5.6	100
27	Spall strength dependence on grain size and strain rate in tantalum. Acta Materialia, 2018, 158, 313-329.	7.9	100
28	The effect of matrix microstructure on the tensile and fatigue behavior of SiC particle-reinforced 2080 Al matrix composites. Metallurgical and Materials Transactions A: Physical Metallurgy and Materials Science, 2000, 31, 531-540.	2.2	93
29	On the correlation between hardness and tensile strength in particle reinforced metal matrix composites. Materials Science & Engineering A: Structural Materials: Properties, Microstructure and Processing, 2001, 297, 44-47.	5.6	90
30	Mechanical Behavior of Multilayered Nanoscale Metal-Ceramic Composites. Advanced Engineering Materials, 2005, 7, 1099-1108.	3.5	90
31	Mechanical behavior and microstructure characterization of sinter-forged SiC particle reinforced aluminum matrix composites. Journal of Light Metals, 2002, 2, 215-227.	0.8	87
32	Thermal expansion anisotropy in extruded SiC particle reinforced 2080 aluminum alloy matrix composites. Materials Science & Engineering A: Structural Materials: Properties, Microstructure and Processing, 2006, 426, 314-322.	5.6	86
33	Thermomechanical behaviour of environmentally benign Pb-free solders. International Materials Reviews, 2009, 54, 368-384.	19.3	86
34	Quantifying the effect of porosity on the evolution of deformation and damage in Sn-based solder joints by X-ray microtomography and microstructure-based finite element modeling. Acta Materialia, 2012, 60, 4017-4026.	7.9	86
35	Micropillar compression of Al/SiC nanolaminates. Acta Materialia, 2010, 58, 6628-6636.	7.9	84
36	3D microstructural characterization and mechanical properties of constituent particles in Al 7075 alloys using X-ray synchrotron tomography and nanoindentation. Journal of Alloys and Compounds, 2014, 602, 163-174.	5.5	84

#	Article	IF	CITATIONS
37	Evaluation of Micro-Pillar Compression Tests for Accurate Determination of Elastic-Plastic Constitutive Relations. Journal of Applied Mechanics, Transactions ASME, 2012, 79, .	2.2	82
38	High temperature micropillar compression of Al/SiC nanolaminates. Acta Materialia, 2013, 61, 4439-4451.	7.9	81
39	Fatigue crack initiation and propagation of binder-treated powder metallurgy steels. Metallurgical and Materials Transactions A: Physical Metallurgy and Materials Science, 2002, 33, 73-81.	2.2	78
40	Deformation analysis of lap-shear testing of solder joints. Acta Materialia, 2005, 53, 2633-2642.	7.9	77
41	An experimental investigation of the fatigue behavior of sisal fibers. Materials Science & Engineering A: Structural Materials: Properties, Microstructure and Processing, 2009, 516, 90-95.	5.6	76
42	Interfacial fracture toughness of Pb-free solders. Microelectronics Reliability, 2009, 49, 269-287.	1.7	76
43	Anisotropy, size, and aspect ratio effects on micropillar compression of Al SiC nanolaminate composites. Acta Materialia, 2016, 114, 25-32.	7.9	75
44	Understanding fatigue crack growth in aluminum alloys by in situ X-ray synchrotron tomography. International Journal of Fatigue, 2013, 57, 79-85.	5.7	74
45	The effects of cooling rate on microstructure and mechanical behavior of Sn-3.5Ag solder. Jom, 2003, 55, 56-60.	1.9	73
46	Indentation behavior of metal–ceramic multilayers at the nanoscale: Numerical analysis and experimental verification. Acta Materialia, 2010, 58, 2033-2044.	7.9	72
47	Microstructure and mechanical behavior of novel rare earth-containing Pb-Free solders. Journal of Electronic Materials, 2006, 35, 2088-2097.	2.2	68
48	Indentation mechanics and fracture behavior of metal/ceramic nanolaminate composites. Journal of Materials Science, 2008, 43, 4383-4390.	3.7	68
49	Mechanisms for Sn whisker growth in rare earth-containing Pb-free solders. Acta Materialia, 2009, 57, 4588-4599.	7.9	68
50	Modeling the effect of particle clustering on the mechanical behavior of SiC particle reinforced Al matrix composites. Journal of Materials Science, 2006, 41, 5731-5734.	3.7	66
51	In situ X-ray synchrotron tomographic imaging during the compression of hyper-elastic polymeric materials. Journal of Materials Science, 2016, 51, 171-187.	3.7	66
52	Modeling and characterizing anisotropic inclusion orientation in heterogeneous material via directional cluster functions and stochastic microstructure reconstruction. Journal of Applied Physics, 2014, 115, .	2.5	64
53	Accurate modeling and reconstruction of three-dimensional percolating filamentary microstructures from two-dimensional micrographs via dilation-erosion method. Materials Characterization, 2014, 89, 33-42.	4.4	63
54	Three-dimensional microstructure characterization of Ag3Sn intermetallics in Sn-rich solder by serial sectioning. Materials Characterization, 2004, 52, 225-230.	4.4	60

#	Article	IF	CITATIONS
55	Numerical simulation of the effect of particle spatial distribution and strength on tensile behavior of particle reinforced composites. Computational Materials Science, 2008, 44, 496-506.	3.0	59
56	On the relationship between solder-controlled and intermetallic compound (IMC)-controlled fracture in Sn-based solder joints. Scripta Materialia, 2012, 66, 586-589.	5.2	58
57	Axial fatigue behavior of binder-treated versus diffusion alloyed powder metallurgy steels. Materials Science & Engineering A: Structural Materials: Properties, Microstructure and Processing, 2001, 308, 180-188.	5.6	57
58	Porous hierarchical TiO2 nanostructures: Processing and microstructure relationships. Acta Materialia, 2009, 57, 854-867.	7.9	57
59	Dendritic morphology of α-Mg during the solidification of Mg-based alloys: 3D experimental characterization by X-ray synchrotron tomography and phase-field simulations. Scripta Materialia, 2011, 65, 855-858.	5.2	56
60	Nanoindentation Behavior of Nanolayered Metal-Ceramic Composites. Journal of Materials Engineering and Performance, 2005, 14, 417-423.	2.5	54
61	Microstructure Characterization and Creep Behavior of Pb-Free Sn-Rich Solder Alloys: Part II. Creep Behavior of Bulk Solder and Solder/Copper Joints. Metallurgical and Materials Transactions A: Physical Metallurgy and Materials Science, 2008, 39, 349-362.	2.2	54
62	Mechanical properties of intermetallic inclusions in Al 7075 alloys by micropillar compression. Intermetallics, 2015, 62, 69-75.	3.9	54
63	Highâ€Frequency Fatigue Behavior of Wovenâ€Fiberâ€Fabricâ€Reinforced Polymerâ€Derived Ceramicâ€Matrix Composites. Journal of the American Ceramic Society, 1998, 81, 1221-1230.	3.8	53
64	Characterization of fatigue behavior of long fiber reinforced thermoplastic (LFT) composites. Materials Characterization, 2009, 60, 537-544.	4.4	53
65	On the Correlation Between Fatigue Striation Spacing and Crack Growth Rate: A Three-Dimensional (3-D) X-ray Synchrotron Tomography Study. Metallurgical and Materials Transactions A: Physical Metallurgy and Materials Science, 2011, 42, 3845-3848.	2.2	53
66	The Effect of Crystallographic Orientation on the Mechanical Behavior of Cu6Sn5 by Micropillar Compression Testing. Journal of Electronic Materials, 2012, 41, 2083-2088.	2.2	53
67	Novel rare-earth-containing lead-free solders with enhanced ductility. Jom, 2006, 58, 57-62.	1.9	52
68	Rate-dependent behavior of Sn alloy–Cu couples: Effects of microstructure and composition on mechanical shock resistance. Acta Materialia, 2012, 60, 4336-4348.	7.9	51
69	Modeling and predicting microstructure evolution in lead/tin alloy via correlation functions and stochastic material reconstruction. Acta Materialia, 2013, 61, 3370-3377.	7.9	51
70	Monotonic and Cyclic Fatigue Behavior of Highâ€Performance Ceramic Fibers. Journal of the American Ceramic Society, 2005, 88, 101-108.	3.8	50
71	Measurement of localized corrosion rates at inclusion particles in AA7075 by in situ three dimensional (3D) X-ray synchrotron tomography. Corrosion Science, 2016, 104, 330-335.	6.6	50
72	Three-dimensional (3D) visualization of reflow porosity and modeling of deformation in Pb-free solder joints. Materials Characterization, 2010, 61, 433-439.	4.4	49

#	Article	IF	CITATIONS
73	Oxidation Behavior of Rare-Earth-Containing Pb-Free Solders. Journal of Electronic Materials, 2009, 38, 210-220.	2.2	48
74	Prediction of bulk tensile behavior of dual phase stainless steels using constituent behavior from micropillar compression experiments. Materials Science & Engineering A: Structural Materials: Properties, Microstructure and Processing, 2012, 534, 220-227.	5.6	48
75	Microstructural evolution and deformation behavior of Al-Cu alloys: A Transmission X-ray Microscopy (TXM) and micropillar compression study. Acta Materialia, 2018, 144, 419-431.	7.9	47
76	Tailoring TiO2 nanotube growth during anodic oxidation by crystallographic orientation of Ti. Scripta Materialia, 2009, 60, 874-877.	5.2	46
77	Growth orientations and morphologies of α-Mg dendrites in Mg–Zn alloys. Scripta Materialia, 2012, 67, 629-632.	5.2	46
78	Fatigue crack growth in SiC particle reinforced Al alloy matrix composites at high and low R-ratios by in situ X-ray synchrotron tomography. International Journal of Fatigue, 2014, 68, 136-143.	5.7	46
79	Microstructure-based modeling of the influence of particle spatial distribution and fracture on crack growth in particle-reinforced composites. Acta Materialia, 2007, 55, 6064-6073.	7.9	45
80	<i>In Situ</i> Investigation of High Humidity Stress Corrosion Cracking of 7075 Aluminum Alloy by Three-Dimensional (3D) X-ray Synchrotron Tomography. Materials Research Letters, 2014, 2, 217-220.	8.7	45
81	Mechanical characterization of microconstituents in a cast duplex stainless steel by micropillar compression. Materials Science & Engineering A: Structural Materials: Properties, Microstructure and Processing, 2014, 598, 98-105.	5.6	45
82	Temperature-dependent mechanical properties of an austenitic–ferritic stainless steel studied by in situ tensile loading in a scanning electron microscope (SEM). Materials Science & Engineering A: Structural Materials: Properties, Microstructure and Processing, 2013, 580, 159-168.	5.6	44
83	3D time-resolved observations of corrosion and corrosion-fatigue crack initiation and growth in peak-aged Al 7075 using synchrotron X-ray tomography. Corrosion Science, 2018, 138, 340-352.	6.6	43
84	Diffusivity and micro-hardness of blended cement materials exposed to external sulfate attack. Cement and Concrete Composites, 2012, 34, 76-85.	10.7	42
85	Microscale deformation behavior of bicrystal boundaries in pure tin (Sn) using micropillar compression. Acta Materialia, 2016, 120, 56-67.	7.9	42
86	In situ experimental techniques to study the mechanical behavior of materials using X-ray synchrotron tomography. Integrating Materials and Manufacturing Innovation, 2014, 3, 109-122.	2.6	41
87	Effect of gallium addition on the microstructure and micromechanical properties of constituents in Nb Si based alloys. Journal of Alloys and Compounds, 2017, 704, 89-100.	5.5	40
88	Three-dimensional (3D) visualization and microstructure-based modeling of deformation in a Sn-rich solder. Scripta Materialia, 2006, 54, 1627-1631.	5.2	39
89	Nanoindentation of rare earth–Sn intermetallics in Pb-free solders. Intermetallics, 2010, 18, 1016-1020.	3.9	39
90	Mechanical properties of metal-ceramic nanolaminates: Effect of constraint and temperature. Acta Materialia, 2018, 142, 37-48.	7.9	39

#	Article	IF	CITATIONS
91	Fatigue crack growth of SiC particle reinforced metal matrix composites. International Journal of Fatigue, 2010, 32, 856-863.	5.7	38
92	Stiffness loss and density decrease due to thermal cycling in an alumina fiber/magnesium alloy composite. Materials Science & Engineering A: Structural Materials: Properties, Microstructure and Processing, 1995, 203, 75-80.	5.6	37
93	The interactive role of inclusions and SiC reinforcement on the high-cycle fatigue resistance of particle reinforced metal matrix composites. Metallurgical and Materials Transactions A: Physical Metallurgy and Materials Science, 2000, 31, 951-957.	2.2	37
94	Three-dimensional (3D) microstructural characterization and quantification of reflow porosity in Sn-rich alloy/copper joints by X-ray tomography. Materials Characterization, 2011, 62, 970-975.	4.4	37
95	Four dimensional (4D) microstructural evolution of Cu6Sn5 intermetallic and voids under electromigration in bi-crystal pure Sn solder joints. Acta Materialia, 2020, 189, 118-128.	7.9	37
96	Microstructure Characterization and Creep Behavior of Pb-Free Sn-Rich Solder Alloys: Part I. Microstructure Characterization of Bulk Solder and Solder/Copper Joints. Metallurgical and Materials Transactions A: Physical Metallurgy and Materials Science, 2008, 39, 340-348.	2.2	36
97	Nanomechanics of biocompatible TiO2 nanotubes by Interfacial Force Microscopy (IFM). Journal of the Mechanical Behavior of Biomedical Materials, 2009, 2, 580-587.	3.1	36
98	Three-Dimensional Microstructure Visualization of Porosity and Fe-Rich Inclusions in SiC Particle-Reinforced Al Alloy Matrix Composites by X-Ray Synchrotron Tomography. Metallurgical and Materials Transactions A: Physical Metallurgy and Materials Science, 2010, 41, 2121-2128.	2.2	36
99	Effect of layer thickness on the high temperature mechanical properties of Al/SiC nanolaminates. Thin Solid Films, 2014, 571, 260-267.	1.8	36
100	Development of a lab-scale, high-resolution, tube-generated X-ray computed-tomography system for three-dimensional (3D) materials characterization. Materials Characterization, 2014, 92, 36-48.	4.4	36
101	Three-dimensional (3D) microstructure visualization of LaSn3 intermetallics in a novel Sn-rich rare-earth-containing solder. Materials Characterization, 2008, 59, 1364-1368.	4.4	35
102	Effect of Rare-Earth (La, Ce, and Y) Additions on the Microstructure and Mechanical Behavior of Sn-3.9Ag-0.7Cu Solder Alloy. Metallurgical and Materials Transactions A: Physical Metallurgy and Materials Science, 2010, 41, 610-620.	2.2	35
103	Electromigration Damage Characterization in Sn-3.9Ag-0.7Cu and Sn-3.9Ag-0.7Cu-0.5Ce Solder Joints by Three-Dimensional X-ray Tomography and Scanning Electron Microscopy. Journal of Electronic Materials, 2014, 43, 33-42.	2.2	35
104	Cyclic Stress-Strain Behavior of Particle Reinforced Metal Matrix Composites. Scripta Materialia, 1998, 38, 1595-1600.	5.2	34
105	Characterization of nanoindentation damage in metal/ceramic multilayered films by transmission electron microscopy (TEM). Materials Science & Engineering A: Structural Materials: Properties, Microstructure and Processing, 2010, 527, 2985-2992.	5.6	34
106	Three dimensional microstructural characterization of nanoscale precipitates in AA7075-T651 by focused ion beam (FIB) tomography. Materials Characterization, 2016, 118, 102-111.	4.4	34
107	Automated correlative segmentation of large Transmission X-ray Microscopy (TXM) tomograms using deep learning. Materials Characterization, 2018, 142, 203-210.	4.4	34
108	Correlating macrohardness and tensile behavior in discontinuously reinforced metal matrix composites. Scripta Materialia, 2000, 42, 427-432.	5.2	33

#	Article	IF	CITATIONS
109	Focused Ion Beam (FIB) tomography of nanoindentation damage in nanoscale metal/ceramic multilayers. Materials Characterization, 2010, 61, 481-488.	4.4	33
110	High-temperature nanoindentation behavior of Al/SiC multilayers. Philosophical Magazine Letters, 2012, 92, 362-367.	1.2	33
111	On the Nature of the Interface between Ag3Sn Intermetallics and Sn in Sn-3.5Ag Solder Alloys. Journal of Electronic Materials, 2007, 36, 1615-1620.	2.2	32
112	Dendritic Growth in Mg-Based Alloys: Phase-Field Simulations and Experimental Verification by X-ray Synchrotron Tomography. Metallurgical and Materials Transactions A: Physical Metallurgy and Materials Science, 2014, 45, 2562-2574.	2.2	32
113	Thermal-shock behavior of a Nicalon-fiber-reinforced hybrid glass-ceramic composite. Composites Science and Technology, 2001, 61, 1923-1930.	7.8	31
114	Effect of overaging and particle size on tensile deformation and fracture of particle-reinforced aluminum matrix composites. Metallurgical and Materials Transactions A: Physical Metallurgy and Materials Science, 2002, 33, 3861-3869.	2.2	31
115	Effect of reinforcement-particle-orientation anisotropy on the tensile and fatigue behavior of metal-matrix composites. Metallurgical and Materials Transactions A: Physical Metallurgy and Materials Science, 2004, 35, 53-61.	2.2	31
116	Characterization of Damage Evolution in SiC Particle Reinforced Al Alloy Matrix Composites by In-Situ X-Ray Synchrotron Tomography. Metallurgical and Materials Transactions A: Physical Metallurgy and Materials Science, 2011, 42, 2999-3005.	2.2	31
117	A microstructure-guided constitutive modeling approach for random heterogeneous materials: Application to structural binders. Computational Materials Science, 2016, 119, 52-64.	3.0	31
118	Mechanical Behavior of Natural Sisal Fibers. Journal of Biobased Materials and Bioenergy, 2010, 4, 106-113.	0.3	31
119	Measurement and prediction of Young's modulus of a Pb-free solder. Journal of Materials Science: Materials in Electronics, 2004, 15, 385-388.	2.2	30
120	Elastic properties of metal–ceramic nanolaminates measured by nanoindentation. Materials Science & Engineering A: Structural Materials: Properties, Microstructure and Processing, 2009, 502, 79-84.	5.6	30
121	Mechanical Characterization of Lead-Free Sn-Ag-Cu Solder Joints by High-Temperature Nanoindentation. Journal of Electronic Materials, 2013, 42, 1085-1091.	2.2	30
122	Micromechanical and in situ shear testing of Al–SiC nanolaminate composites in a transmission electron microscope (TEM). Materials Science & Engineering A: Structural Materials: Properties, Microstructure and Processing, 2015, 621, 229-235.	5.6	30
123	Stochastic Multi-Scale Reconstruction of 3D Microstructure Consisting of Polycrystalline Grains and Second-Phase Particles from 2D Micrographs. Metallurgical and Materials Transactions A: Physical Metallurgy and Materials Science, 2016, 47, 1440-1450.	2.2	30
124	Effect of porosity and tension–compression asymmetry on the Bauschinger effect in porous sintered steels. International Journal of Fatigue, 2005, 27, 1233-1243.	5.7	29
125	Mechanical properties of a thermally-aged cast duplex stainless steel by nanoindentation and micropillar compression. Materials Science & Engineering A: Structural Materials: Properties, Microstructure and Processing, 2019, 743, 520-528.	5.6	29
126	Multiscale investigation of corrosion damage initiation and propagation in AA7075-T651 alloy using correlative microscopy. Corrosion Science, 2021, 185, 109429.	6.6	29

#	Article	IF	CITATIONS
127	Electromigration mechanisms in Sn-0.7Cu/Cu couples by four dimensional (4D) X-ray microtomography and electron backscatter diffraction (EBSD). Acta Materialia, 2016, 102, 220-230.	7.9	28
128	3D X-ray microtomography and mechanical characterization of corrosion-induced damage in 7075 aluminium (Al) alloys. Corrosion Science, 2018, 139, 97-113.	6.6	28
129	Surface roughness characterization of Nicalonâ,,¢ and HI-Nicalonâ,,¢ ceramic fibers by atomic force microscopy. Materials Characterization, 1995, 35, 199-206.	4.4	27
130	An evaluation of the lap-shear test for Sn-rich solder/Cu couples: Experiments and simulation. Journal of Electronic Materials, 2004, 33, 1589-1595.	2.2	27
131	Thermal Fatigue Behavior of Sn-Rich (Pb-Free) Solders. Metallurgical and Materials Transactions A: Physical Metallurgy and Materials Science, 2008, 39, 799-810.	2.2	27
132	Multiscale microstructural characterization of Sn-rich alloys by three dimensional (3D) X-ray synchrotron tomography and focused ion beam (FIB) tomography. Materials Characterization, 2012, 70, 33-41.	4.4	27
133	Direct extraction of spatial correlation functions from limited x-ray tomography data for microstructural quantification. Materials Characterization, 2018, 140, 265-274.	4.4	27
134	Three Dimensional (3D) Microstructural Characterization and Quantitative Analysis of Solidified Microstructures in Magnesium-Based Alloys. Metallography, Microstructure, and Analysis, 2012, 1, 7-13.	1.0	26
135	Deformation mechanisms of ultra-thin Al layers in Al/SiC nanolaminates as a function of thickness and temperature. Philosophical Magazine, 2016, 96, 3336-3355.	1.6	26
136	In Situ X-ray Microtomography of Stress Corrosion Cracking and Corrosion Fatigue in Aluminum Alloys. Jom, 2017, 69, 1404-1414.	1.9	26
137	Quantifying Electrochemical Reactions and Properties of Amorphous Silicon in a Conventional Lithium-Ion Battery Configuration. Chemistry of Materials, 2017, 29, 5831-5840.	6.7	26
138	Analysis of indentation-derived effective elastic modulus of metal-ceramic multilayers. International Journal of Mechanics and Materials in Design, 2008, 4, 391-398.	3.0	25
139	Mechanical behavior of NiTi shape memory alloy fiber reinforced Sn matrix "smart―composites. Journal of Materials Science, 2009, 44, 700-707.	3.7	25
140	Fatigue crack growth behavior of hybrid and prealloyed sintered steels. Materials Science & Engineering A: Structural Materials: Properties, Microstructure and Processing, 2008, 491, 28-38.	5.6	24
141	Mechanical properties of microconstituents in Nb-Si-Ti alloy by micropillar compression and nanoindentation. Materials Science & Engineering A: Structural Materials: Properties, Microstructure and Processing, 2017, 687, 99-106.	5.6	24
142	The role of interfacial coatings on the high frequency fatigue behavior of nicalon/C/SiC composites. Scripta Materialia, 1996, 35, 1411-1416.	5.2	23
143	Hybrid and conventional particle reinforced metal matrix composites by squeeze infiltration casting. Journal of Materials Science Letters, 2002, 21, 337-339.	0.5	23
144	Effect of residual surface stress on the fatigue behavior of a low-alloy powder metallurgy steel. International Journal of Fatigue, 2007, 29, 1978-1984.	5.7	23

#	Article	IF	CITATIONS
145	Interfacial Reactions in Model NiTi Shape Memory Alloy Fiber-Reinforced Sn Matrix "Smart― Composites. Metallurgical and Materials Transactions A: Physical Metallurgy and Materials Science, 2009, 40, 176-184.	2.2	23
146	Digital image correlation analysis of the deformation behavior of Pb-free solders at intermediate strain rates. Jom, 2010, 62, 16-21.	1.9	23
147	Residual stress characterization of Al/SiC nanoscale multilayers using X-ray synchrotron radiation. Thin Solid Films, 2010, 519, 759-765.	1.8	23
148	Environmental Effects on Fatigue Crack Growth in 7075 Aluminum Alloy. Metallurgical and Materials Transactions A: Physical Metallurgy and Materials Science, 2012, 43, 2799-2809.	2.2	23
149	Image analysis of cracks in the weld metal of a wet welded steel joint by three dimensional (3D) X-ray microtomography. Materials Characterization, 2013, 83, 139-144.	4.4	23
150	Creep deformation behavior of Sn-3.5Ag solder at small length scales. Jom, 2004, 56, 50-54.	1.9	22
151	Scratch resistance of Al/SiC metal/ceramic nanolaminates. Journal of Materials Research, 2012, 27, 278-283.	2.6	22
152	Multiscale 3D characterization of discontinuities in underwater wet welds. Materials Characterization, 2015, 107, 358-366.	4.4	22
153	A Forward Modeling Approach to High-Reliability Grain Mapping by Laboratory Diffraction Contrast Tomography (LabDCT). Jom, 2019, 71, 2695-2704.	1.9	22
154	Xâ€Ray Microtomography of Thermal Cycling Damage in Sintered Nanoâ€Silver Solder Joints. Advanced Engineering Materials, 2019, 21, 1801029.	3.5	22
155	3D Time-Resolved Observations of Fatigue Crack Initiation and Growth from Corrosion Pits in Al 7XXX Alloys Using In Situ Synchrotron X-ray Tomography. Metallurgical and Materials Transactions A: Physical Metallurgy and Materials Science, 2020, 51, 28-41.	2.2	22
156	Bauschinger effect in porous sintered steels. Materials Science & Engineering A: Structural Materials: Properties, Microstructure and Processing, 2003, 346, 266-272.	5.6	21
157	Cyclic indentation behavior of metal–ceramic nanolayered composites. Materials Science & Engineering A: Structural Materials: Properties, Microstructure and Processing, 2012, 557, 119-125.	5.6	21
158	Mechanical shock behavior of Sn–3.9Ag–0.7Cu and Sn–3.9Ag–0.7Cu–0.5Ce solder joints. Microelectronics Reliability, 2013, 53, 733-740.	1.7	21
159	Characterisation of thermal cycling induced cavitation in particle reinforced metal matrix composites by three-dimensional (3D) X-ray synchrotron tomography. Materials Science and Technology, 2015, 31, 573-578.	1.6	21
160	Exploring novel deformation mechanisms in aluminum–copper alloys using in situ 4D nanomechanical testing. Acta Materialia, 2019, 176, 242-249.	7.9	21
161	Direct observations of microstructure-resolved corrosion initiation in AA7075-T651 at the nanoscale using vertical scanning interferometry (VSI). Materials Characterization, 2020, 161, 110166.	4.4	21
162	Reconstruction of heterogeneous materials via stochastic optimization of limited-angle X-ray tomographic projections. Scripta Materialia, 2014, 86, 48-51.	5.2	20

#	Article	IF	CITATIONS
163	Probing Novel Microstructural Evolution Mechanisms in Aluminum Alloys Using 4D Nanoscale Characterization. Advanced Materials, 2017, 29, 1703482.	21.0	20
164	Hierarchical n-point polytope functions for quantitative representation of complex heterogeneous materials and microstructural evolution. Acta Materialia, 2019, 179, 317-327.	7.9	20
165	The cyclic fatigue of high-performance fibers. Jom, 2005, 57, 67-71.	1.9	19
166	Microstructure-based modeling of deformation in Sn-rich (Pb-free) solder alloys. Journal of Materials Science: Materials in Electronics, 2006, 18, 175-189.	2.2	19
167	Thermal and Mechanical Stability of Ce-Containing Sn-3.9Ag-0.7Cu Lead-Free Solder on Cu and Electroless Ni-P Metallizations. Journal of Electronic Materials, 2012, 41, 3249-3258.	2.2	18
168	Influence of Thermal Aging on the Microstructure and Mechanical Behavior of Dual-Phase, Precipitation-Hardened, Powder Metallurgy Stainless Steels. Metallurgical and Materials Transactions A: Physical Metallurgy and Materials Science, 2012, 43, 124-135.	2.2	18
169	Fractography of a neck failure in a double-modular hip implant. Case Studies in Engineering Failure Analysis, 2014, 2, 45-50.	1.2	18
170	Microstructure and nanoindentation of the rostrum of Curculio longinasus Chittenden, 1927 (Coleoptera: Curculionidae). Materials Characterization, 2016, 118, 206-211.	4.4	18
171	Analysis of thermal history effects on mechanical anisotropy of 3D-printed polymer matrix composites via in situ X-ray tomography. Journal of Materials Science, 2017, 52, 12185-12206.	3.7	18
172	Mechanisms of deformation in high-ductility Ce-containing Sn–Ag–Cu solder alloys. Microelectronics Reliability, 2011, 51, 1142-1147.	1.7	17
173	Evolution of mechanical, optical and electrical properties of self-assembled mesostructured phenolic resins during carbonization. Microporous and Mesoporous Materials, 2011, 138, 86-93.	4.4	17
174	Modeling Fracture of Sn-Rich (Pb-Free) Solder Joints Under Mechanical Shock Conditions. Journal of Electronic Materials, 2012, 41, 2089-2099.	2.2	17
175	Accurate stochastic reconstruction of heterogeneous microstructures by limited xâ€ray tomographic projections. Journal of Microscopy, 2016, 264, 339-350.	1.8	17
176	Granule formation and structure from single drop impact on heterogeneous powder beds. International Journal of Pharmaceutics, 2018, 552, 56-66.	5.2	17
177	Three dimensional (3D) microstructure-based finite element modeling of Al-SiC nanolaminates using focused ion beam (FIB) tomography. Materials Characterization, 2016, 120, 369-376.	4.4	16
178	Modeling Anisotropic Multiphase Heterogeneous Materials via Directional Correlation Functions: Simulations and Experimental Verification. Metallurgical and Materials Transactions A: Physical Metallurgy and Materials Science, 2012, 43, 4470-4474.	2.2	15
179	Extracting Constitutive Stress–Strain Behavior of Microscopic Phases by Micropillar Compression. Jom, 2013, 65, 226-233.	1.9	15
180	Mechanical Behavior of Particle Reinforced Metal Matrix Composites. Advanced Engineering Materials, 2001, 3, 357-370.	3.5	15

#	Article	IF	CITATIONS
181	Finite element simulation of swelling-induced crack healing in gels. Soft Matter, 2012, 8, 8107.	2.7	14
182	Mechanisms of Sn Hillock Growth in Vacuum by InÂSitu Nanoindentation in a Scanning Electron Microscope (SEM). Journal of Electronic Materials, 2013, 42, 224-229.	2.2	14
183	Three dimensional modeling of complex heterogeneous materials via statistical microstructural descriptors. Integrating Materials and Manufacturing Innovation, 2014, 3, 25-43.	2.6	14
184	A multilayer micromechanical model of the cuticle of Curculio longinasus Chittenden, 1927 (Coleoptera: Curculionidae). Journal of Structural Biology, 2016, 195, 139-158.	2.8	14
185	Orientation dependence of indentation behavior in Al–SiC nanolaminate composites. Materials Letters, 2016, 168, 129-133.	2.6	14
186	Machine-Learning-based Algorithms for Automated Image Segmentation Techniques of Transmission X-ray Microscopy (TXM). Jom, 2021, 73, 2173-2184.	1.9	14
187	Rheology scaling of spherical metal powders dispersed in thermoplastics and its correlation to the extrudability of filaments for 3D printing. Additive Manufacturing, 2021, 41, 101967.	3.0	14
188	Effect of laminate stacking sequence on the high frequency fatigue behavior of SCS-6 fiber-reinforced Si3N4 matrix composites. Metallurgical and Materials Transactions A: Physical Metallurgy and Materials Science, 1997, 28, 2423-2427.	2.2	13
189	Fatigue crack growth behavior of hybrid and prealloyed sintered steels. Materials Science & Engineering A: Structural Materials: Properties, Microstructure and Processing, 2008, 491, 19-27.	5.6	13
190	Microstructure and mechanical properties of co-sputtered Al-SiC composites. Materials and Design, 2019, 168, 107670.	7.0	13
191	Electromigration in Bi-crystal pure Sn solder joints: Elucidating the role of grain orientation. Journal of Alloys and Compounds, 2020, 818, 152918.	5.5	13
192	Plastic deformation during indentation unloading in multilayered materials. Journal of Applied Physics, 2008, 104, 116102.	2.5	12
193	The Effect of Random Voids in the Modified Gurson Model. Journal of Electronic Materials, 2012, 41, 177-183.	2.2	12
194	Enhancing the Ductility of Sn-Ag-Cu Lead-Free Solder Joints by Addition of Compliant Intermetallics. Journal of Electronic Materials, 2013, 42, 527-536.	2.2	12
195	A Study of Pb-Rich Dendrites in a Near-Eutectic 63Sn-37Pb Solder Microstructure via Laboratory-Scale Micro X-ray Computed Tomography (μXCT). Journal of Electronic Materials, 2014, 43, 4442-4456.	2.2	12
196	Note: Design and construction of a multi-scale, high-resolution, tube-generated X-Ray computed-tomography system for three-dimensional (3D) imaging. Review of Scientific Instruments, 2014, 85, 016103.	1.3	12
197	Microstructure and micropore formation in a centrifugally-cast duplex stainless steel via X-ray microtomography. Materials Characterization, 2019, 148, 52-62.	4.4	12
198	Micromechanical properties and deformation behavior of Al3BC/6061 Al composites via micropillar compression. Materials Science & Engineering A: Structural Materials: Properties, Microstructure and Processing, 2020, 773, 138852.	5.6	12

#	Article	IF	CITATIONS
199	Bioinspired Honeycomb Core Design: An Experimental Study of the Role of Corner Radius, Coping and Interface. Biomimetics, 2020, 5, 59.	3.3	12
200	Influence of Substrate Surface Finish Metallurgy on Lead-Free Solder Joint Microstructure with Implications for Board-Level Reliability. Journal of Electronic Materials, 2020, 49, 3251-3258.	2.2	12
201	Shockâ€wave synthesis of a thalliumâ€based superconductor with a novel defect microstructure. Applied Physics Letters, 1989, 55, 2339-2341.	3.3	11
202	Localized compression and shear tests on nanotargets with a Berkovich tip and a novel multifunctional tip. Journal of Materials Research, 2009, 24, 768-775.	2.6	11
203	Microstructureâ€Based Modeling of Deformation in Steels Based on Constitutive Relationships from Micropillar Compression. Steel Research International, 2014, 85, 946-953.	1.8	11
204	Mechanisms of thermal cycling damage in polycrystalline Sn-rich solder joints. Materials Science & Engineering A: Structural Materials: Properties, Microstructure and Processing, 2020, 771, 138614.	5.6	11
205	Synchrotron CT imaging of lattice structures with engineered defects. Journal of Materials Science, 2020, 55, 11353-11366.	3.7	11
206	Ligand Crosslinking Boosts Thermal Transport in Colloidal Nanocrystal Solids. Angewandte Chemie - International Edition, 2020, 59, 9556-9563.	13.8	11
207	Tensile and fracture behavior of silica fibers from the Venus flower basket (Euplectella aspergillum). International Journal of Solids and Structures, 2022, 253, 111622.	2.7	11
208	Parametric optimization of corner radius in hexagonal honeycombs under in-plane compression. Journal of Manufacturing Processes, 2022, 79, 35-46.	5.9	11
209	The Comparative Approach to Bio-Inspired Design: Integrating Biodiversity and Biologists into the Design Process. Integrative and Comparative Biology, 2022, 62, 1153-1163.	2.0	11
210	Explosive shock-compression processing of titanium aluminide/titanium diboride composites. Journal of Materials Science, 1991, 26, 232-240.	3.7	10
211	Effect of cerium addition on wetting, undercooling, and mechanical properties of Sn-3.9Ag-0.7Cu Pb-free solder alloys. Journal of Materials Science: Materials in Electronics, 2013, 24, 3456-3466.	2.2	10
212	Rapid method for testing efficacy of nano-engineered coatings for mitigating tin whisker growth. Microelectronics Reliability, 2015, 55, 832-837.	1.7	10
213	Full elastic constants of Cu 6 Sn 5 intermetallic by Resonant Ultrasound Spectroscopy (RUS) and ab initio calculations. Scripta Materialia, 2015, 107, 26-29.	5.2	10
214	Nanoscale Three-Dimensional Microstructural Characterization of an Sn-Rich Solder Alloy Using High-Resolution Transmission X-Ray Microscopy (TXM). Microscopy and Microanalysis, 2016, 22, 808-813.	0.4	10
215	In situ tensile testing of tin (Sn) whiskers in a focused ion beam (FIB)/scanning electron microscope (SEM). Microelectronics Reliability, 2017, 79, 314-320.	1.7	10
216	Synchrotron-Based X-ray Computed Tomography During Compression Loading of Cellular Materials. Microscopy Today, 2015, 23, 12-19.	0.3	9

#	Article	IF	CITATIONS
217	In situ micropillar compression of Al/SiC nanolaminates using laboratory-based nanoscale X-ray microscopy: Effect of nanopores on mechanical behavior. Materials Characterization, 2019, 150, 207-212.	4.4	9
218	Nucleation and Growth of Tin Hillocks by In Situ Nanoindentation. Journal of Electronic Materials, 2019, 48, 58-71.	2.2	9
219	Nanomechanical characterization of the fracture toughness of Al/SiC nanolaminates. Extreme Mechanics Letters, 2020, 40, 100945.	4.1	9
220	Chromophoreâ€Free Sealing and Repair of Soft Tissues Using Midâ€Infrared Lightâ€Activated Biosealants. Advanced Functional Materials, 2021, 31, 2007811.	14.9	9
221	Microstructural Coarsening and Mechanical Properties of Eutectic Sn-58Bi Solder Joint During Aging. Journal of Electronic Materials, 2021, 50, 6607-6614.	2.2	9
222	Thermo-mechanical characterization of 2080 Al/SiCp composites by mechanical spectroscopy technique. Journal of Materials Science Letters, 2001, 20, 163-166.	0.5	8
223	Mechanical Shock Behavior of Bulk Pure Sn Solder. Journal of Electronic Materials, 2009, 38, 2746-2755.	2.2	8
224	Effect of fiber fabric orientation on the flexural monotonic and fatigue behavior of 2D woven ceramic matrix composites. Materials Science & Engineering A: Structural Materials: Properties, Microstructure and Processing, 2012, 557, 77-83.	5.6	8
225	Fracture Behavior of Sn-3.5Ag-0.7Cu and Pure Sn Solders as a Function of Applied Strain Rate. Journal of Electronic Materials, 2012, 41, 2519-2526.	2.2	8
226	Quantifying necking of rectangular tensile specimens using a mirror-based image analysis system. Materials Letters, 2012, 74, 243-246.	2.6	8
227	Tensile Behavior of Single-Crystal Tin Whiskers. Journal of Electronic Materials, 2014, 43, 978-982.	2.2	8
228	Highâ€Temperature Micropillar Compression Creep Testing of Constituent Phases in Leadâ€Free Solder. Advanced Engineering Materials, 2015, 17, 1168-1174.	3.5	8
229	Activation Energy for End-of-Life Solder Bond Degradation: Thermal Cycling of Field-Aged PV Modules. IEEE Journal of Photovoltaics, 2020, 10, 1762-1771.	2.5	8
230	Three-dimensional (3D) microstructure-based modeling of crack growth in particle reinforced composites. Journal of Materials Science, 2007, 42, 9125-9129.	3.7	7
231	Effect of Mounting Material Compliance on Nanoindentation Response of Metallic Materials. Advanced Engineering Materials, 2009, 11, 45-51.	3.5	7
232	Multiscale Modeling of the Interfacial Fracture Behavior in the Sn–Cu ₆ Sn ₅ –Cu System. Journal of Computational and Theoretical Nanoscience, 2011, 8, 873-880.	0.4	7
233	Anomalous viscoplasticity during nanoindentation of Al/SiC nanolaminated composites. Materials Science & Engineering A: Structural Materials: Properties, Microstructure and Processing, 2011, 528, 4608-4614.	5.6	7
234	Avoidance of Catastrophic Structural Failure as an Evolutionary Constraint: Biomechanics of the Acorn Weevil Rostrum. Advanced Materials, 2019, 31, 1903526.	21.0	7

#	Article	IF	CITATIONS
235	In situ X-ray microtomography of the compression behaviour of eTPU bead foams with a unique graded structure. Journal of Materials Science, 2021, 56, 5082-5099.	3.7	7
236	The interactive role of inclusions and SiC reinforcement on the high-cycle fatigue resistance of particle reinforced metal matrix composites. Metallurgical and Materials Transactions A: Physical Metallurgy and Materials Science, 2000, 31, 951-957.	2.2	6
237	Three-dimensional (3D) modeling of the thermoelastic behavior of woven glass fiber-reinforced resin matrix composites. Journal of Materials Science, 2008, 43, 6468-6472.	3.7	6
238	Two-dimensional microstructure based modelling of Young's modulus of long fibre thermoplastic composite. Materials Science and Technology, 2008, 24, 864-869.	1.6	6
239	Processing and microstructure characterization of a novel porous hierarchical TiO2 structure. Journal of Materials Research, 2009, 24, 1683-1687.	2.6	6
240	Flocculated carbon nanotube composites for solvent resistant soft templated microfeatures. Polymer, 2013, 54, 1130-1135.	3.8	6
241	Three Dimensional Characterization of Tin Crystallography and Cu6Sn5 Intermetallics in Solder Joints by Multiscale Tomography. Jom, 2016, 68, 2879-2887.	1.9	6
242	Microstructural Quantification and Property Prediction Using Limited X-ray Tomography Data. Jom, 2016, 68, 2288-2295.	1.9	6
243	Data Challenges of In Situ X-Ray Tomography for Materials Discovery and Characterization. Springer Series in Materials Science, 2018, , 129-165.	0.6	6
244	3D grain structure of an extruded 6061 Al alloy by lab-scale X-ray diffraction contrast tomography (DCT). Materials Characterization, 2020, 170, 110716.	4.4	6
245	Effect of Trace Addition of In on Sn-Cu Solder Joint Microstructure Under Electromigration. Journal of Electronic Materials, 2021, 50, 893-902.	2.2	6
246	X-ray computer tomography (XCT) of fatigue damage in laser-machined versus milled carbon fiber reinforced polymer matrix composites. Engineering Fracture Mechanics, 2021, 252, 107820.	4.3	6
247	Three Dimensional (3D) Visualization of Damage in Metal-Ceramic Nanolayers by Focused Ion Beam (FIB) Serial Sectioning. Microscopy and Microanalysis, 2008, 14, 140-141.	0.4	5
248	On the Asymmetric Growth Behavior of Intermetallic Compound Layers During Extended Reflow of Sn-Rich Alloy on Cu. Metallurgical and Materials Transactions A: Physical Metallurgy and Materials Science, 2012, 43, 3442-3446.	2.2	5
249	Efficient methods for implicit geometrical representation of complex material microstructures. International Journal for Numerical Methods in Engineering, 2014, 98, 79-91.	2.8	5
250	Modeling and characterization of X-ray yield in a polychromatic, lab-scale, X-ray computed tomography system. Nuclear Instruments and Methods in Physics Research, Section A: Accelerators, Spectrometers, Detectors and Associated Equipment, 2015, 783, 110-116.	1.6	5
251	Hydrogen permeability and mechanical properties of NiNb-M (MÂ=ÂSn, Ti and Zr) amorphous metallic membranes. Journal of Alloys and Compounds, 2016, 684, 359-365.	5.5	5
252	Crack bridging modelling in Bioglass ® based scaffolds reinforced by poly-vinyl alcohol/microfibrillated cellulose composite coating. Mechanics of Materials, 2017, 110, 16-28.	3.2	5

#	Article	IF	CITATIONS
253	Powder bed packing and API content homogeneity of granules in single drop granule formation. Powder Technology, 2020, 366, 12-21.	4.2	5
254	Poisson's ratio of eTPU molded bead foams in compression via in situ synchrotron X-ray microtomography. Journal of Materials Science, 2021, 56, 12920-12935.	3.7	5
255	4D microstructural characterization of corrosion and corrosion-fatigue in a Ti–6Al–4V / AA 7075-T651 joint in saltwater environment. Materials Science & Engineering A: Structural Materials: Properties, Microstructure and Processing, 2021, 825, 141886.	5.6	5
256	Continuous Nanoparticle Patterning Strategy in Layer‣tructured Nanocomposite Fibers. Advanced Functional Materials, 2022, 32, .	14.9	5
257	A multi-scale investigation of the mechanical behavior of durable sisal fiber cement composites. Revista Materia, 2010, 15, 338-344.	0.2	4
258	Tensile and Fatigue Behavior of Al-1Si Wire Used in Wire Bonding. Journal of Electronic Materials, 2011, 40, 1422-1427.	2.2	4
259	Electrochemical Mechanical Removal of Ta Films in Dihydroxybenzene Sulfonic Acid Solutions Containing Potassium Iodate. Electrochemical and Solid-State Letters, 2011, 14, H156.	2.2	4
260	Effect of Component Flexibility During Thermal Cycling of Sintered Nano-Silver Joints by X-ray Microtomography. Journal of Electronic Materials, 2020, 49, 241-244.	2.2	4
261	Computational Imaging in 3D X-Ray Microscopy: Reconstruction, Image Segmentation and Time-Evolved Experiments. , 2021, , .		4
262	Data intensive science at synchrotron based 3D x-ray imaging facilities. , 2012, , .		3
263	Fatigue and fracture of powder metallurgy steels. , 2013, , 455-490.		3
264	A method for zinger artifact reduction in high-energy x-ray computed tomography. Nuclear Instruments and Methods in Physics Research, Section A: Accelerators, Spectrometers, Detectors and Associated Equipment, 2015, 800, 82-92.	1.6	3
265	In situ fixture for multi-modal characterization during electromigration and thermal testing of wire-like microscale specimens. Microelectronics Reliability, 2015, 55, 2345-2353.	1.7	3
266	Microstructural characterization and mechanical property prediction of a polymer matrix composite by X-ray synchrotron tomography and spatial correlation functions. SN Applied Sciences, 2019, 1, 1.	2.9	3
267	<i>In situ</i> Four Dimensional (4D) X-ray Microtomography of the Compressive Behavior of eTPU Foam for High Performance Footware. Microscopy and Microanalysis, 2019, 25, 364-365.	0.4	3
268	Mechanical properties of Al3BC by nanoindentation and micropillar compression. Materials Letters, 2020, 264, 127361.	2.6	3
269	Reducing the risk of rostral bending failure in Curculio Linnaeus, 1758. Acta Biomaterialia, 2021, 126, 350-371.	8.3	3

270 Mechanical Behavior of Particle Reinforced Metal Matrix Composites. , 2001, 3, 357.

3

#	Article	IF	CITATIONS
271	In Situ Three Dimentional (3D) X-Ray Synchrotron Tomography of Corrosion Fatigue in Al7075 Alloy. , 2013, , 17-25.		3
272	Processing. , 2013, , 55-97.		3
273	Predicting the Cu6Sn5 Growth Kinetics During Thermal Aging of Cu-Sn Solder Joints Using Simplistic Kinetic Modeling. Journal of Electronic Materials, 2022, 51, 4063-4072.	2.2	3
274	The fracture toughness and fatigue behavior of DRA. Jom, 1999, 51, 69-72.	1.9	2
275	Fatigue of Particle Reinforced Materials. , 2001, , 2967-2971.		2
276	A Self-Consistent Approach for Necking Correction in Tensile Specimens With Rectangular Cross-Section Using a Novel Mirror Fixture. Metallurgical and Materials Transactions A: Physical Metallurgy and Materials Science, 2012, 43, 5058-5066.	2.2	2
277	Characterization and Adhesion in Cu/Ru/SiO2/Si Multilayer Nano-scale Structure for Cu Metallization. Journal of Materials Engineering and Performance, 2013, 22, 1085-1090.	2.5	2
278	A study of EM failure in a micro-scale Pb-free solder joint using a custom lab-scale x-ray computed tomography system. , 2014, , .		2
279	Geometry segmentation of voxelized representations of heterogeneous microstructures using betweenness centrality. Materials Characterization, 2016, 118, 553-559.	4.4	2
280	1.1 Fibrous Reinforcements for Composites. , 2018, , 1-12.		2
281	In situ Imaging of Materials using X-ray Tomography. Microscopy and Microanalysis, 2018, 24, 1002-1003.	0.4	2
282	Three-Dimensional (3D) Microstructure-Based Modeling of a Thermally-Aged Cast Duplex Stainless Steel Based on X-ray Microtomography, Nanoindentation and Micropillar Compression. Metals, 2019, 9, 688.	2.3	2
283	Unveiling the deformation behavior and strengthening mechanisms of Al3BC/Al composites via in-situ micropillar compression. Journal of Alloys and Compounds, 2020, 823, 153842.	5.5	2
284	Ligand Crosslinking Boosts Thermal Transport in Colloidal Nanocrystal Solids. Angewandte Chemie, 2020, 132, 9643-9650.	2.0	2
285	Microstructure-based modeling of deformation in Sn-rich (Pb-free) solder alloys. , 2006, , 175-189.		2
286	Processing of Ceramic-Matrix Composites. , 2001, , 589-599.		2
287	Structure and Defects of Shock-Processed Ti and Y-Based Copper Oxide Superconductors. Materials Research Society Symposia Proceedings, 1990, 183, 381.	0.1	1
288	Mechanical and electrical issues concerning the use of composite materials for the supporting core in transmission line conductors. , 2006, , .		1

0

#	Article	IF	CITATIONS
289	Multiscale modeling of composite materials. Jom, 2008, 60, 38-38.	1.9	1
290	Applying Pattern Recognition to the Analysis of X-ray Computed Tomography Data of Polymer Foams. Microscopy and Microanalysis, 2016, 22, 104-105.	0.4	1
291	Understanding Nanoscale 4D Microstructural Evolution in Aluminum Alloys using Transmission X-Ray Microscopy (TXM). Microscopy and Microanalysis, 2017, 23, 2220-2221.	0.4	1
292	Multimodal 3D Time-Lapse Studies of Corrosion Pitting and Corrosion-Fatigue Behavior in 7475 Aluminum Alloys. Microscopy and Microanalysis, 2017, 23, 324-325.	0.4	1
293	Creep. , 2013, , 283-309.		1
294	Novel Hierarchical Correlation Functions for Quantitative Representation of Complex Heterogeneous Materials and Microstructural Evolution. SSRN Electronic Journal, 0, , .	0.4	1
295	Monotonic and Cyclic Fatigue Behavior of a High Performance Ceramic Fiber. Materials Research Society Symposia Proceedings, 2001, 702, 1.	0.1	0
296	Preface to special section on composite materials. Journal of Materials Science, 2008, 43, 4353-4355.	3.7	0
297	In-situ Compression Imaging of Polymer Foams using Synchrotron X-ray Computed Tomography. Microscopy and Microanalysis, 2014, 20, 672-673.	0.4	0
298	Micro-scale X-ray Computed Tomography of Additively Manufactured Cellular Materials under Uniaxial Compression. Microscopy and Microanalysis, 2015, 21, 129-130.	0.4	0
299	Automated Correlative Tomography of an Aluminum 7075 Alloy Spanning Length Scales and Modalities. Microscopy and Microanalysis, 2015, 21, 1345-1346.	0.4	0
300	Effective Constitutive Response of Sustainable Next Generation Infrastructure Materials through High-Fidelity Experiments and Numerical Simulation. Procedia Engineering, 2017, 173, 1258-1265.	1.2	0
301	Probing Material Morphology and Deformation as a Response to in situ Loading using X-ray Tomography. Microscopy and Microanalysis, 2019, 25, 374-375.	0.4	0
302	3D/4D X-Ray Microtomography: Probing the Mechanical Behavior of Materials. , 2019, , 2013-2033.		0
303	Fracture Analysis of Particulate Metal Matrix Composite Using X-ray Tomography and Extended Finite Element Method (XFEM). Journal of Composites Science, 2020, 4, 62.	3.0	0
304	Reinforcements. , 2013, , 5-36.		0
305	Cyclic Fatigue. , 2013, , 227-282.		0

306 3D/4D X-Ray Microtomography: Probing the Mechanical Behavior of Materials. , 2018, , 1-21.